JMEPEG (2007) 16:229–235
DOI: 10.1007/s11665-007-9037-z

1059-9495/$19.00

Effect of Mg Content on the Performance of Al-Zn-Mg Sacrificial Anodes

R. Orozco, J. Genesca and J. Juarez-Islas

(Submitted January 3, 2005; in revised form December 16, 2005)

Aluminum sacrificial anodes are widely used in cathodic protection of steel structures in sea water. In the present work, samples of Al-5.3 at.% Zn-*x* at.% Mg (*x* = 5.5-8.5) alloys were microstructurally and electrochemically characterized to evaluate their performance as Al-sacrificial anodes for cathodic protection of structures exposed to marine environments. The experiments focussed on the influence of Mg content on electrochemical behavior and efficiency. Mg was used in different concentrations ranging from 5.5 to 8.5 at.%. Short-term electrochemical tests, DNV RP B401, as well as polarization curves and electrochemical impedance spectroscopy were performed to obtain electrochemical behavior and efficiency and to reveal any tendencies to passivation. It is shown that by increasing Mg content an improvement of electrochemical properties of Al-alloy such as current capacity and then electrochemical efficiency can be obtained.

Keywords casting, current efficiency, electrochemical reactions, electrode materials, sacrificial anodes

1. Introduction

Aluminum galvanic anodes are used for corrosion protection of various marine structures such as offshore platforms, ship hulls, etc. Aluminum alloys suitable for cathodic protection have been developed in recent years, and the influence of alloying elements such as zinc (Zn), titanium (Ti), mercury (Hg), and indium (In) has been studied by several researchers (Ref 1-2). Many works refer to the addition of Hg, gallium (Ga), tin (Sn), and In to aluminum alloys. Each of these elements has been demonstrated to improve aluminum activation in neutral chloride media; however, the good results obtained in this field clash with the increased sensitivity to environmental protection. Particularly the use of Hg (which may be dangerous during the manufacture of the sacrificial anodes), pollutes sea-life, thus giving rise to great concern about the environment. Research towards the substitution of dangerous elements such as Hg involves the scientific knowledge of solidification processing, the kinetics precipitation of primary binary/ternary intermetallics, the distribution of intermetallics and/or precipitates in α-Al solid solution after heat treatment, and the corrosion mechanisms involved during the dissolution of this kind of anode.

Technical knowledge involves the melting/casting of aluminum alloys with ternary additions of elements belonging to the groups IIA and IIB from the periodic table, and the implementation of electrochemical techniques which are adequate for the evaluation of the current efficiency of the anode.

It has been reported out (Ref 3) that in Al-IIB-IIA system, the α-Al solid solution and the τ-phase with a composition close to the $Al_2IIA_3IIB_3$ are present (Ref 4). In the as-cast condition the main microstructure is formed by the α-Al solid solution and the second phase τ (Ref 4). The eutectic formed by a fine dispersion of the α + τ is segregated at grain boundaries and to some extent the τ-phase is partially dispersed in the core of the aluminum grains. To promote further fine dispersion of the τ-phase in the matrix, thermal treatments can be carried out on the resulting ingots by taking advantage of the fast kinetic reactions occurring in the solid state. The addition of a combination of IIA and IIB elements in Al is carried out with the aim of assuring that the aluminum oxide does not develop protective properties against dissolution, being the amount and distribution of intermetallic compounds relevant on the electrochemical and corrosion behavior of the alloy.

With reference to the Al-IIB-IIA ternary phase diagram (Ref 5), in the isotherm at 400 °C (720 °F), there is present the α-Al solid solution plus eutectic of the Al_2IIA_3IIB, which ensure via aging treatments a fine dispersion of this eutectic which help the non-passivation of the anode. In order to make the Al-Zn-Mg ternary system more efficient with respect to the superficial activation of the anode (preventing the formation of superficial aluminum oxide films) additions of IA are convenient (Ref 6) with the aim of precipitating the Al_3IA (δ') in matrix, by taking advantage of the fact that the Zn lowest the solid solubility of IA in the α-Al phase and also of the fact that Zn can be incorporated to the δ' phase. This has been the subject of a previous research (Ref 7).

This research has as its main objective the electrochemical testing of the Al-IIB-IIA type alloys in order to be used as aluminum sacrificial anodes. The choice of the alloy system has as its basis the precipitation and distribution of fine intermetallic phases belonging to the ternary Al-IIB-IIA system, in the α-Al matrix, with the aim of achieving two ends: (1) a good surface activation of the anode and, (2) formation of corrosion

R. Orozco and **J. Genesca,** Dpto. Ingenieria Metalúrgica, Facultad Química, UNAM, Ciudad Universitaria, 04510 Mexico, DF, Mexico; and **J. Juarez-Islas,** Instituto Investigación en Materiales, UNAM, Ciudad Universitaria, 04510 DF, Mexico. Contact e-mail: genesca@servidor.unam.mx

Table 1 Alloy compositions and electrochemical efficiency of the alloys under study

Alloy	Field	Zn, at.%	Mg, at.%	Si, at.%	Cu, at.%	Al	ε (as-cast)
1	(C^{eq}_{max})	5.3	5.3	0.168	0.003	Bal.	68
2	α + τ	5.3	6.7	0.160	0.002	Bal.	73
3	α + τ	5.3	7.2	0.125	0.008	Bal.	73
4	α + τ	5.3	11.3	0.152	0.002	Bal.	78

ε: electrochemical efficiency, %

products similar to those found in the salts of the sea water, thus preventing the pollution of sea life.

2. Experimental Procedure

Al, Zn, and Mg elements of commercial purity (99.5%), previously weighed, were placed into a SiC crucible and melted into a resistance furnace under an argon protective atmosphere. The liquid melt was gravity cast into a steel chill mold of dimensions 3.08 cm × 3.08 cm. The resulting alloys showed compositions (Table 1), which lie in the maximum concentration of solute at equilibrium (C^{eq}_{max}) and in the α + τ field. The resulting ingots were cut out in sections parallel to the heat flow. The microstructure was revealed by electroetching the samples (25 V, −10 °C, 20 s) in a solution containing 10% perchloric acid, $HClO_4$, in ethanol, CH_3CH_2OH. The samples were observed under an optical (Zeiss-Olympus) and scanning electron (Stereoscan 440) microscopes.

Electrochemical impedance measurements were conducted by using a Gill AC potentiostat from ACM Instruments over a frequency range of 10 kHz to 100 mHz (10 points per decade) superimposing a 10 mV AC signal. Potentiodynamic polarization curves were carried out with a Gill AC potentiostat at a sweep rate of 60 mV/min.

3. Experimental Results and Discussion

The structure observed in chill-cast ingots showed the presence of dendrites and eutectic in interdendritic regions, as that is shown in Fig. 1. During solidification of the alloys, the first phase to growth was the α-Al, which developed a dendritic pattern. As the solidification continued, the liquid surrounding the advancing solid/liquid interface was enriched with solute (Zn and Mg) and as the temperature dropped and reached a phase transformation, phases such as the τ-phase and the eutectic (α + τ) were formed. Regarding the τ-phase (reported previously (Ref 3) to be a key factor to promote a good surface activation of the anode avoiding the formation of the continuous, adherent and protective oxide film on the alloy surface, once in service), this was mainly observed in the specimens with 5.3 at.% Zn + 6.7, 7.2 and 11.3 at.% Mg.

A representative microstructure observed in the as-cast ingot, Fig. 1, consisted of α-Al dendrites. In the interdendritic regions, the presence of an eutectic was observed.

A short-term electrochemical test, DNV RP B 401 (Ref 8) was performed on these Al-Zn-Mg alloys. Cubic anodes were machined from the ingot, thus eliminating the structure formed by direct contact with the mold wall. The accelerated electrochemical test was carried out to determine anode efficiency and working potential (Ref 8). All potentials were measured relative to a saturated calomel reference electrode (SCE). Samples were held galvanostatically at different current density levels. Each level was applied during a 24-h period. The total duration of the test was 96 h. During the test, the anode potential was measured at the beginning and at the end of each current density level period (every 24 h). This could reveal any tendencies to passivation. The test solution was aerated substitute ocean water with an initial pH 8.3 according to ASTM D1141 (Ref 9).

The calculated electrochemical efficiency (Ref 8), ε, for the as-cast Al anode samples was 68%, corresponding approximately to 2026 A · h/kg (the lowest efficiency reached in the alloys under study). The closed-circuit potentials measured

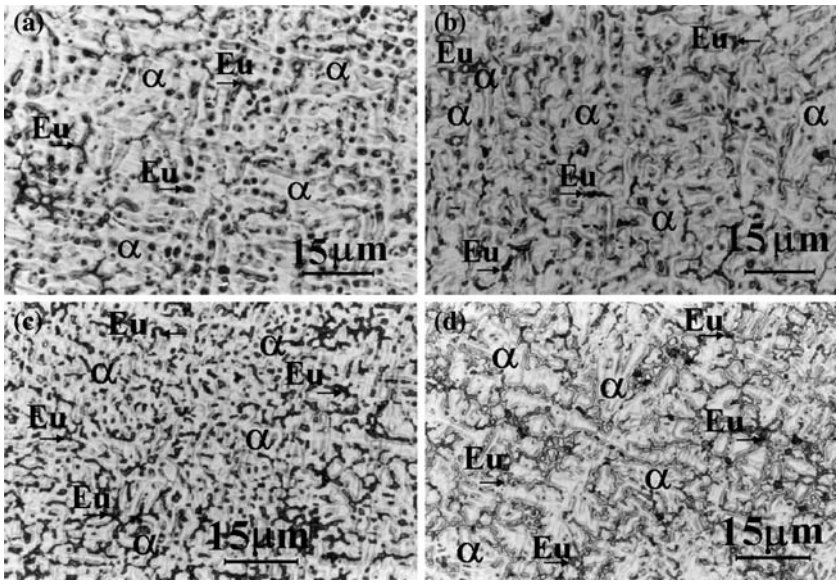

Fig. 1 Microstructure observed in chill-cast ingots of Al-Zn-Mg alloys. (a) Al-5.3 at.% Zn-5.3 at.% Mg, (b) Al-5.3 at.% Zn-6.7 at.% Mg, (c) Al-5.3 at.% Zn-7.2 at.% Mg, and (d) Al-5.3 at.% Zn-11.3 at.% Mg

were in the range between −1.05 V (SCE) and −1.15 V (SCE). An active closed-circuit potential is desirable because a relatively noble potential could indicate the presence of passivation. Anodes must also possess high faradic efficiency to prevent frequent anode replacement. The NACE (Ref 10) and DNV (Ref 8) tests specify that an Al anode should have a closed-circuit potential active to −1.0 V (SCE) and a ε between 2300 and 2700 A · h/kg. Then the anode analyzed met the potential criterion, but appeared to exhibit only moderate efficiency. Theoretically, uniform anode dissolution will give maximum efficiency. Either secondary cathodic reaction on the same interface and/or mechanical grain loss due to local macro or microcorrosion cells will reduce the anode efficiency (Ref 11). In Al-Zn alloys, Zn tends to be rejected to interdendritic zones or grain boundaries. This effect is favored by the cooling rate and the alloying element characteristics (lower melting point than aluminum). Under polarization, this local composition variation will favor the initiation and propagation of macro- and micro-local events (galvanic corrosion and pitting for example). These events are responsible for lowering anode efficiency by electrochemical or mechanical mass loss (Ref 11). The low efficiencies showed by the studied anodes are similar to those obtained by Salinas et al. (Ref 11) for Al-5% Zn alloy. A possible explanation is that the main efficiency loss can be ascribed to the secondary reactions, since they are produced by the relatively high content of impurities, particularly Fe and Cu, that cause local cell action.

Regarding the Al-Zn-Mg alloys, it is reported in the literature (Ref 12) that a τ-phase exists in equilibrium with a solid solution of Mg and Zn in Al (α-solid solution). The $Al_2Mg_3Zn_3$ phase exists in a range of compositions which could be useful in obtaining the depolarization feature of the alloys. The structure of the studied aluminum-alloys has been recognized as composed of two phases: the α-Al matrix in which Mg and Zn are present to some extent, and the ternary intermetallic compound (phase τ). The formation and distribution of the intermetallic phase in the aluminum matrix in the form of many small crystals have been promoted as a key factor in achieving good surface activation of the anode. Then, electrochemical efficiency must increase when volume content of τ-phase increases. The investigation of the effect of this intermetallic on the activation capability of Al-Zn-Mg alloys when exposed to an aggressive environment containing chlorides has been carried out. The electrochemical efficiency (Table 1) clearly showed how these aluminum alloys are strongly affected by the presence and amount of this type of intermetallic. From X-ray phase analysis (Ref 13) it has been possible to demonstrate that τ-phase can be formed on the alloys which composition is away from equilibrium.

To obtain more information about the effect of Mg content on the electrochemical efficiency, a new set of experiments was carried out. Table 2 shows the chemical composition of these Al-alloys. Electrochemical efficiency was determined as previously indicated (Ref 8).

The microstructure and microanalysis of these new set of alloys is shown in Fig. 2.

3.1 Corrosion Potential, E_{corr}

The corrosion potential variation as a function of immersion time is shown in Fig. 3. For all the Al-alloys and independently of Mg content, corrosion potential shifts to more negative potentials, ranging from −1010 to −1045 mV (SCE). As the anode is consumed the zones with different alloying elements are exposed, which lead to variation of corrosion potential with time and non-uniform dissolution of anode occurs. Previous works with similar alloys but with lower Mg contents showed E_{corr} potentials in the range between −1012 and −1017 mV (SCE) (Ref 3, 14-17).

Table 2 Alloy compositions and electrochemical efficiency of the alloys under study

Alloy	Zn, at.%	Mg, at.%	Si, wt.%	Cu, wt.%	Al	ε (as-cast)
5.5 Mg	5.30	5.48	0.0575	0.0060	bal.	72
6.5 Mg	5.33	6.61	0.0797	0.0093	bal.	73
7.5 Mg	5.37	7.47	0.0870	0.0099	bal.	69
8.5 Mg	5.34	8.51	0.0657	0.0072	bal.	75

ε: electrochemical efficiency, %

3.2 Potentiodynamic Sweep Measurements

The effect of Mg content on the polarization behavior of these alloys is shown in Fig. 4. Addition of Mg to the anode alloy shifts the corrosion potential to more negative values, which is desirable for cathodic protection systems. The potentiodynamic polarization plots of Al-Zn-Mg alloys show that the anodic behavior looks very similar, and in all the cases no passivation was observed on the anodic parts of the curve, but the cathodic behavior presents some important differences as a function of Mg content.

The cathodic behavior seems to be interpreted as follows: a first activation region near E_{corr}, followed by a diffusion area, possibly due to oxygen reduction at intermediate potentials, and finally a new activation region at higher potentials due to the water reduction. It is clear that the Al-5.3Zn-8.5Mg alloy shows an important catalytic effect of the surface elements on oxygen reduction reaction. At 8.5% Mg more negative potential and lowering in O_2 reduction limiting current can be observed.

Polarization curves for the four alloys are shown in Fig. 4 for the experimental conditions studied. These polarization curves were obtained in a 3% NaCl solution at 20 °C. The polarization curves showed in Fig. 4 indicate that, in general, a good reproducibility was obtained in the experimental results. Referring to the anodic branch of the polarization curves, almost three main regions can be observed:

- One first region developing from the E_{corr} to potential values of −0.99 V (SCE),
- A second region in which a sudden change on the slope of the anodic current occurs, between −0.99 and −0.93 V (SCE),
- Finally, a third region at higher anodic potentials, where another change on the slope of the anodic curve can be observed. This region can be seen above −0.93 V (SCE).

These features can be explained in a qualitative manner as follows. As the potential of the working electrode increases from E_{corr}, an anodic reaction on the Al-alloy surface occurs and a linear relationship between the applied potential and the logarithm of the current density can be observed which corresponds to a charge-transfer process known as Tafel region, characterized by a slope, Tafel slope, which contains mechanistic information about the corrosion reaction. In the region in

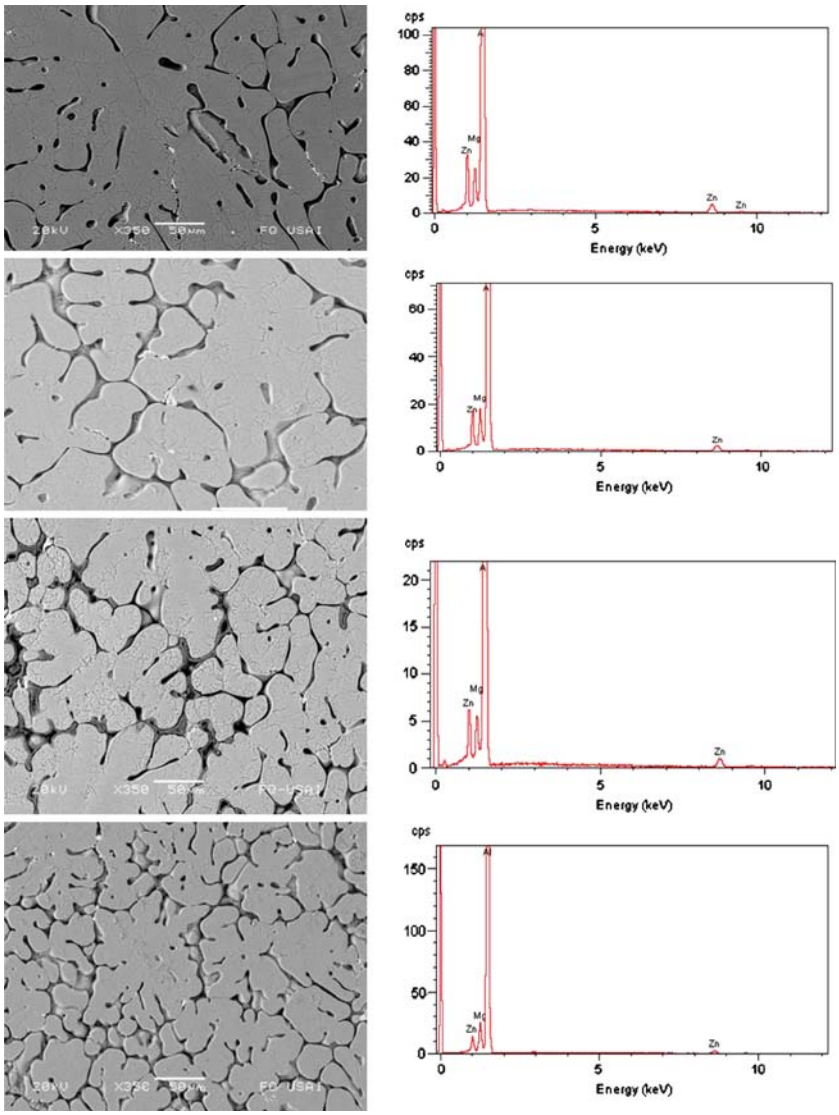

Fig. 2 SEM images of microstructure and EDS analysis of the Al-5.3Zn-*x*Mg (x = 5.5-8.5%) anode samples in the as-cast condition

which a sudden change on the slope of the anodic polarization curve occurs with a plateau in the anodic current, this behavior can be attributed to the formation of a pseudo-passivating film. This film could be due to the formation of a Al_2O_3 layer on the metal surface. At higher anodic potentials the resulting anodic current density increases again. This may be attributed to the growth of the film previously formed.

Aluminum reacts readily with Cl^- in aqueous solutions containing NaCl. Hence one might hypothesize that the native barrier oxide is gradually converted to a hydrated salt film at the oxide solution interface. Figure 4 illustrates dc polarization results on Al-Zn-Mg alloy as a function of Mg content. All data are IR corrected. For 8.5% Mg content the polarization behavior seems to be consistent with the notion that the native Al_2O_3 is converted to a non-protective $AlCl_3 \times H_2O$ film. A white gel-like film was observed. After the 336 h of immersion time, the morphology of the corrosion products formed on the surface of Al-alloys was observed in the MEB, Fig. 5(a). X-ray microanalysis clearly shows the formation of a possible aluminum hydroxychloride, $Al_2O_3 \cdot xAlCl_3 \cdot yH_2O$.

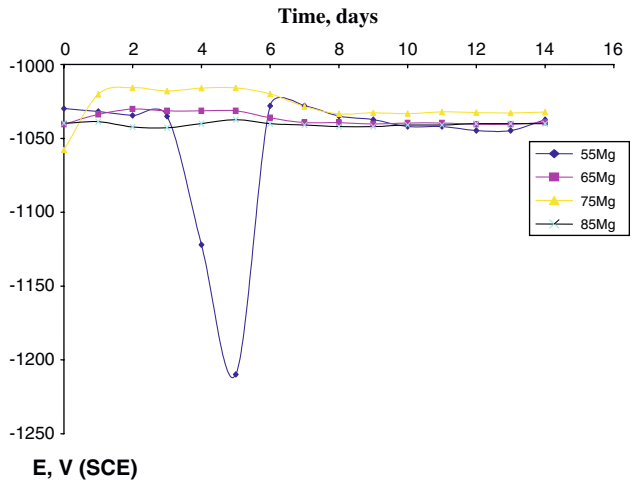

Fig. 3 Corrosion potential, E_{corr} as a function of immersion time

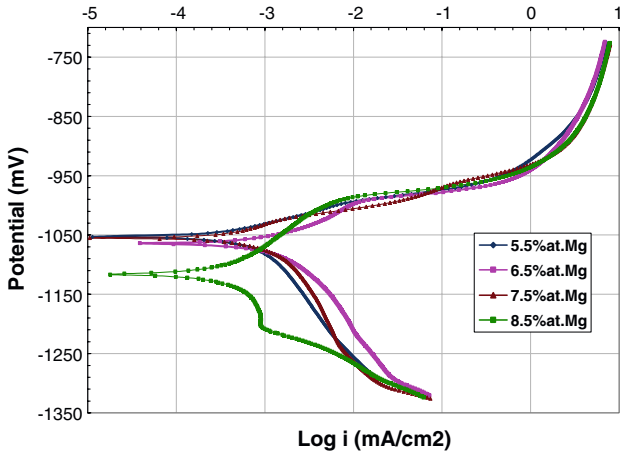

Fig. 4 Potentiodynamic polarization curves of Al-5.3%Zn-*x*Mg (*x* = 5.5-8.5%) in 3% NaCl at room temperature

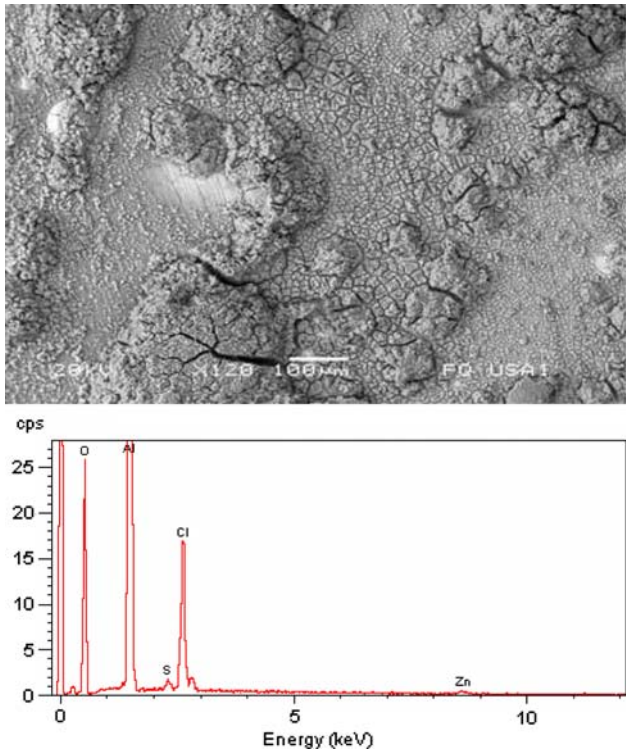

Fig. 5 MEB and EDAX analysis of corrosion products formed after 336 h of immersion

3.3 Electrochemical Impedance Spectroscopy (EIS) Measurements

With EIS it is possible to monitor the conversion of the native oxide-covered metal to $AlCl_3$ covered with both exposure time and increasing Mg content. EIS also provides a means to verify the presence of oxide at the most lower Mg content. Figure 6(a) and (b) illustrate the experimental impedance response at E_{corr} potential. Electrochemical impedance spectroscopy measurements were performed as a function of immersion time. The shape of the diagrams shows, independently of Mg content, the presence of one capacitive semicircle. By increasing immersion time, Fig. 6(b), a second time-

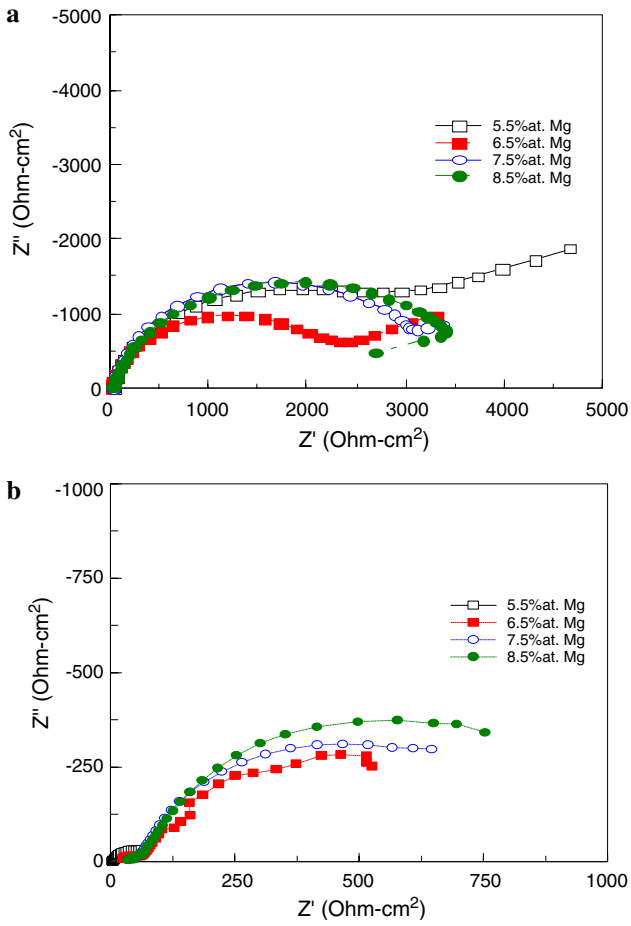

Fig. 6 EIS diagrams of Al-5.3Zn-*x*Mg (*x* = 5.5-8.5%) anode samples in 3% NaCl at room temperature. (a) After immersion, (b) after 336 h of immersion

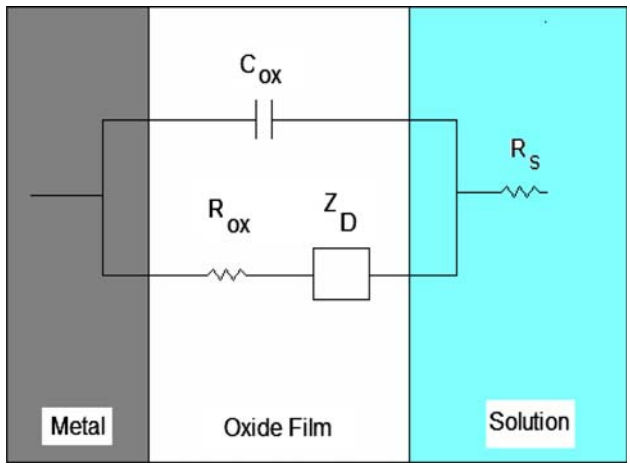

Fig. 7 Electric equivalent circuit

constant at high frequency begins to develop, that could be due to the formation of a layer of corrosion products. The capacitive behavior at high and medium frequencies might be due to the corrosion products film and the metal/oxide interface. EIS fit was obtained assuming the equivalent circuit model illustrated in Fig. 7, which correspond to the classic mass

transfer control. According to this model, oxides are characterized by a high-frequency parallel RC network consisting of the oxide capacitance in parallel with the oxide resistance and a low-frequency diffusional impedance associated with anion and cation transport across the oxide. The oxide impedance is proportional to oxide thickness and inversely proportional to the ability of the oxide to support both electronic and ionic charge transfer across the oxide. The low-frequency EIS response associated with the diffusional impedance of the oxide depends on the Warburg coefficient for both anions and cations, σ. The justification for choosing this particular model is based on previous work on oxide-covered metals in the literature (Ref 18, 19).

Concerning the high-frequency EIS response, the capacitance obtained by EIS is, in principle, given by the oxide film capacitance, C_{ox}, in series with the double-layer capacitance at the oxide/solution interface, C_{dl} (Ref 18, 20):

$$\frac{1}{C_t} = \frac{1}{C_{ox}} + \frac{1}{C_{dl}} \quad \text{(Eq 1)}$$

where C_{ox} is given by

$$C_{ox} = \varepsilon\varepsilon_0 \frac{1}{d_{ox}} \quad \text{(Eq 2)}$$

$d_{ox}$is the oxide thickness and other terms have their usual meaning. C_{ox} is approximately 16.42 μF/cm^2 just after exposure which yields a 0.54-nm-thick Al_2O_3 film from Eq 2 assuming ε = 5-10.

Since C_{dl} is normally 40-60 μF/cm^2, C_t is dominated by C_{ox} in Eq 1 for a homogeneous oxide-covered surface.

R_{ox} and C_t are shown in Fig. 8 and 9 as a function of exposure time at E_{corr} potential for the different Mg content indicated. Capacitance data indicate thinning of the native barrier oxide with increasing exposure time since:

(a) C_t at short exposure times is in good agreement with initial oxide thicknesses calculated using Eq 2, and
(b) C_t increases with exposure time indicative of oxide thinning and exposure of bare metal.

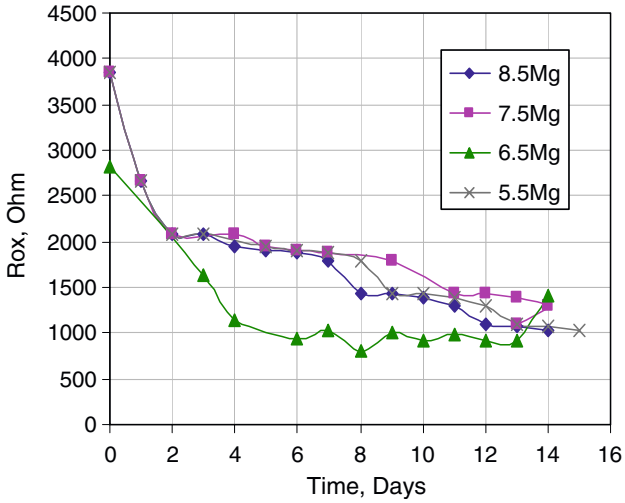

Fig. 8 Corrosion products resistance, R_{ox} as a function of immersion time

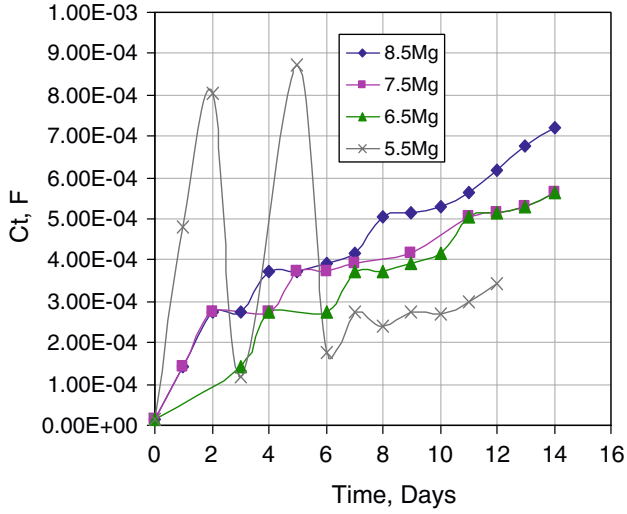

Fig. 9 Capacitance, C_t as a function of immersion time

Note that C_t increases with increasing Mg content, Fig. 9, while R_{ox} decreases, Fig. 8, and that the low-frequency diffusional impedance is no longer observed at 7.5% Mg, Fig. 6(a). These results further substantiate the claim that the low-frequency EIS response observed in Fig. 6(a) is indeed attributed to a diffusional impedance associated with the oxide since the conversion of the oxide to a gel-like salt resulted in the suppression of the low-frequency diffusional impedance response. The data in Fig. 8 indicate that the native oxide is dissolved and converted to a salt film within about 12 days.

4. Conclusions

As-cast Al-5.3Zn-Mg alloys showed a microstructure that consisted of α-Al dendrites and eutectic α + τ in interdendritic regions. This alloy reached values of electrochemical efficiency up to 75%.

Magnesium addition helps in improving the anode current capacity when present to the extent of 8.5%.

Acknowledgments

This work was supported by a grant from CONACYT (Mexico) (Project NC-204) and SECRETARIA MARINA (MARINA-2002-C01-1553). One of the authors, R. Orozco wishes to thank CONACYT for a Ph.D. grant.

References

1. A.R. Despić, D.M. Dražić, M.M. Purenović, and N. Ciković, Electrochemical Proiperties of Aluminium Alloys Containing Indium, Gallium and Thallium, *J. Appl. Electrochem.*, 1976, **6**(6), p 527–542
2. M.M.B.H. Salleh, Ph.D. Thesis, Institute of Science and Technology, Victoria University of Manchester, Manchester, 1978
3. A. Barbucci, G. Cerisola, G Bruzzone, and A. Saccone, Activation of Aluminium Anodes by the Presence of Intermetallic Compounds, *Electrochim. Acta*, 1997, **42**(15), p 2369–2380
4. R.J. Kilmer and G.E. Stoner, Effect of Trace Additions of Zn on the Precipitation Behavior of Alloy 8090 During Artificial Aging, *Light-Weight Alloys for Aerospace Applications II*, TMS, 1991, p 2–15

5. D.A. Petrov, Aluminium-Magnesium-Zinc, in *Ternary Alloys*, G. Petzow and G. Effenberg, Eds. VCH, Weinheim, 1993, p 57–71
6. X. Zhand and Y. Wang, *Corr. Sci. Prot.* (*China*), Vol 7 (No. 1), 1995, p 53
7. M.A. Talavera, S. Valdez, B. Mena, J.A. Juarez-Islas, and J. Genesca, EIS Testing of New Aluminium Sacrificial Anodes, *J. Appl. Electrochem.*, 2002, **32**, p 8897–8903
8. "Cathodic Protection Design," DNV Recommended Practice RP B401, Det Norske Veritas Industry AS, Hovik, 1993
9. "Standard Practice for the Preparation of Substitute Ocean Water," ASTM D 1141, *Book of Standards Volume: 11:02*, ASTM International, www.astm.org
10. "Impressed Current Laboratory Testing of Aluminum Alloy Anodes," NACE Standard Test Method 0190-98, NACE International, Houston, 1998
11. D.R. Salinas, S.G. Garcia, and J.B. Bessone, Influence of Alloying Elements and Microstructure on Aluminium Sacrificial Anode Performance: Case of Al-Zn, *J. Appl. Electrochem.*, 1999, **29**(9), p 1063–1071
12. G. Bruzzone, A. Barbucci, and G. Cerisola, Effect of Intermetallic Compounds on the Activation of Aluminium Anodes, *J. Alloy Compd.*, 1997, **247**(1–2), p 210–216
13. C. Gonzalez, O. Alvarez, J. Genesca, and J.A. Juarez-Islas, Solidification of Chill-Cast Al-Zn-Mg Alloys to be Used as Sacrificial Anodes, *Metall. Mater. Trans.*, 2003, **34A**(12), p 2991–2997
14. R. Orozco-Cruz, J. Genesca, and J.A. Juarez-Islas, "Desarrollo y evaluación electroquímica de una aleación Al-Zn-Mg" ("Development and Electrochemical Evalution of an Al-Zn-Mg Alloy"), *XVIIIth Congress of the Mexican Society of Electrochemistry, Topic 1*, Paper # T1.8P, Chihuahua, 2003
15. J.B. Clark, Phase Relations in the Magnesium-Rich Region of the Mg-Al-Zn Phase Diagram, *Trans. Am. Soc. Met.*, 1961, **53**, p 295–306
16. R.T. Foley and P.P. Trzaskoma, *Passivity of Metals*, R.P. Frankental and J. Kruger, Eds., The Electrochemical Society, New Jersey, 1978, p 337
17. M.A. Talavera, S. Valdez, J.A. Juarez-Islas, and J. Genesca, "Development and Testing of Aluminum Sacrificial Anodes In/Hg Free," Paper # 01508, Corrosion/2001, NACE International, Houston, 2001
18. J. R. Scully, *Electrochemical Impedance: Analysis and Interpretation*, J.R. Scully, D.C. Silverman, and M.W. Kendig, Eds., ASTM STP 1188, Philadelphia, 1993, p 276–296
19. D.D. MacDonald, R.Y. Liang, and B.G. Pound, An Electrochemical Impedance Study of the Passive Film on Single Crystal Ni (111) in Phosphate Solutions, *J. Electrochem. Soc.*, 1987, **134**(12), p 2981–2986
20. J.W. Diggle, *Oxides and Oxide Films*. Vol. I, Marcel Dekker, New York, 1972, p 319-517